Covalent Molecular Assembly in a Supercritical Medium: Formation of Nanoparticles Encapsulated in Immobilized Dendrimers

ARTICLE *in* INDUSTRIAL & ENGINEERING CHEMISTRY RESEARCH · DECEMBER 2006

Impact Factor: 2.59 · DOI: 10.1021/ie060822q

2 AUTHORS:

Sreenivasa Reddy Puniredd
Agency for Science, Technology and Researc…
48 PUBLICATIONS **770** CITATIONS
SEE PROFILE

Madapusi P Srinivasan
RMIT University
168 PUBLICATIONS **2,643** CITATIONS
SEE PROFILE

Covalent Molecular Assembly in a Supercritical Medium: Formation of Nanoparticles Encapsulated in Immobilized Dendrimers

Sreenivasa Reddy Puniredd and M. P. Srinivasan*

Department of Chemical and Biomolecular Engineering, National University of Singapore, 4 Engineering Drive 4, Singapore 117576

This work demonstrates the feasibility of forming metallic nanoparticles within the confines of dendrimer-laden ultrathin films that are immobilized on a solid surface. The functional property of the poly amido amine dendrimer (PAMAM) as a sequestering agent for Cu nanoparticles was exploited by the introduction of copper acetylacetonate ($Cu(acac)_2$) as a precursor. The nanoparticle precursors were introduced into the matrix using supercritical carbon dioxide and liquid tetrahydrofuran (THF) as processing media. The precursors were subsequently reduced to form the nanoparticles. The resulting film assemblies were characterized via X-ray photoelectron and UV−visible absorption spectroscopies, atomic force, scanning electron, transmission electron microscopies, and ellipsometry. Higher yield, a denser distribution of nanoparticles, and greater stability toward polar solvent attack were observed when the structures were assembled in supercritical CO_2 than when THF was employed. TEM images revealed that the embedded nanoparticles are fairly tightly distributed in terms of size with an average diameter of 7 nm.

1. Introduction

Controlling the particle size and distribution is a critical issue for applications involving nanoparticles. For sensing, catalysis, and other applications involving electronic and optical properties,[1,2] it is also necessary to immobilize the nanoparticles on a solid support. Templating techniques for immobilizing nanoparticles on to surfaces involve creation of electrostatic interactions[3−5] or covalent bonds[6−9] between the nanoparticle and the surface. Additionally, with the objective of forming particles with controlled size and distribution, dendrimers have been used as templates for preparing metallic, bimetallic, and semiconductor nanoparticles.[10−12] Dendrimer-encapsulated metal nanoparticles are prepared typically by a two-step process: the metal precursors are sequestered within the dendrimer, and then the precursors are chemically/thermally reduced. Because the synthesis relies on dendrimeric templates, the resulting metal nanoparticles can be monodispersed in size.

The preparation of a range of Cu, Pd, Pt, Ag, and Au metallic nanoparticles with dendrimers as templates has been reported.[13−18] The properties of metal−dendrimer nanocomposites depend on the nature of the terminal groups of the dendrimers. Amine peripheral groups are able to induce agglomeration and precipitation of large metal clusters.[19] This may be caused by the complexation of many metal precursors with the periphery of amine-terminated dendrimers, which typically results in formation of nanosized metal clusters stabilized by multiple dendrimers.[20]

Tripathy et al. reported the electrostatic LbL assembly of gold−dendrimer nanoclusters.[21] In a similar work, Luo et al. reported the assembly of ultrathin films forming Ag−PAMAM dendrimer nanocomposites.[22] Pd and Pt nanoparticles prepared within dendrimers have been immobilized onto Au surfaces via covalent amide bond formation between the unquaternized amine groups on the dendrimer periphery and anhydride-activated self-assembled monolayers (SAMs).[23]

In the reports mentioned above, a solvent in the liquid state is typically used as the processing medium, especially to convey the precursor to the dendrimer-containing matrix. However, the viscosity of the liquid retards penetration into narrow spaces or pores. Even when gaseous phases under their critical temperatures are used, capillary condensation may occur in fine spaces. Such problems may be avoided and penetration of the dendrimer matrix promoted when a material in the supercritical state is used, on account of its relatively lower viscosity and higher diffusivity.

Interest in using carbon dioxide in its supercritical state ($SCCO_2$) is stimulated by the environmentally benign nature of CO_2 in comparison with the organic solvents used in technological processes. It is widely applied as a carrier in impregnation[24,25] and polymer synthesis.[26] It has been used for formation of self-assembled monolayers of alkanethiols on gold surfaces,[27,28] self-assembled structures of block copolymers,[29] and synthesis of nanoparticles such as Ag, Pt, Pd, Ir, and Ag−Pd from their organometallic precursors in $SCCO_2$.[30,31] Preparation of Pt nanoparticles in poly(4-methyl-1-pentene) and poly(tetrafluroethylene),[32−34] Ag nanoparticles on the surface of polyimide film,[35,36] poly(styrene-divinylbenzene),[37] and poly(etherether ketone)[38] and Pt−Pd nanocomposite in carbon molecular sieves(CMS),[39] using $SCCO_2$ have been reported. However, there is little information in published literature about using $SCCO_2$ as a processing medium for dendrimers.[40]

While sequestration of nanoparticles in regular confined spaces such as dendrimeric systems and immobilization of nanoparticles on surfaces have been separately demonstrated, our present work focuses on immobilizing the sequestering agent (dendrimer) in thin film systems formed by covalent molecular assembly followed by formation of the nanoparticle within the immobilized dendrimer matrix. It would be of much interest, for example, in catalysis, to be able to anchor catalytically active nanoparticles in porous matrices using dendrimeric components as sequestering agents.[41] It would be of interest also to know whether the use of $SCCO_2$ for impregnating the matrix with the precursor would result in the attendant benefits expected of the supercritical medium, its advantageous transport and solubility properties, being manifested in the size and distribution of the nanoparticles formed in the matrix.

* To whom correspondence should be addressed. Tel.: +65-65162171. Fax: +65-67791936. E-mail: chesmp@nus.edu.sg.

10.1021/ie060822q CCC: $37.00
Published on Web 12/09/2006

Chart 1. Experimental Setup for the SCF Process

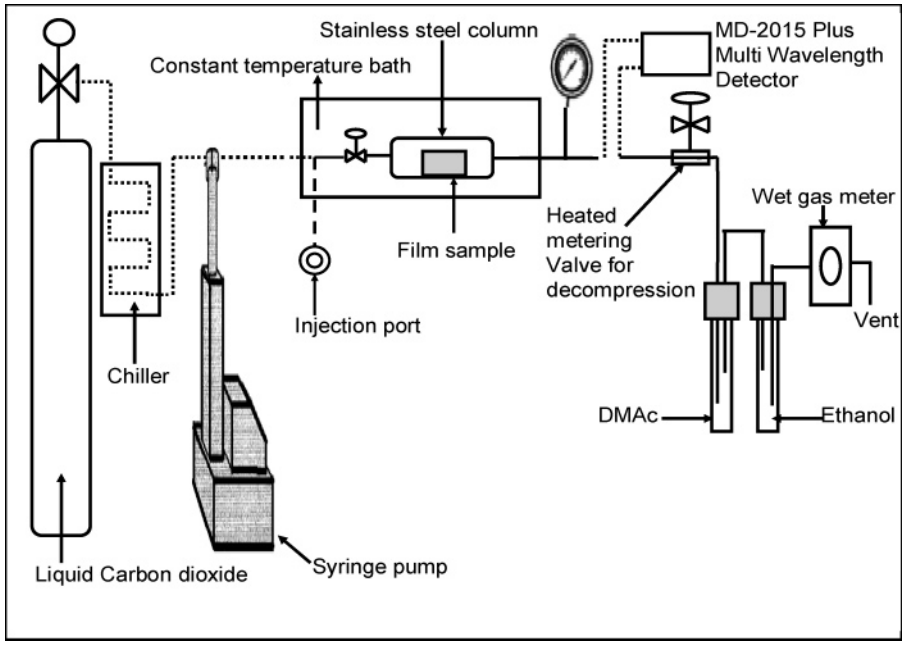

Recently, we showed that the $SCCO_2$ could be used as a vehicle for building ultrathin films of oligoimide on silicon dioxide surface.[42,43] The quality of the films in SCF medium was better than that for films formed in *N*,*N*-dimethylacetamide (DMAc), and the SCF-grown films were mechanically and thermally more stable. We have also investigated the formation of covalently bonded, multilayered, dendrimer-containing ultrathin films consisting of PAMAM and PMDA (pyromellitic dianhydride) using supercritical carbon dioxide as a vehicle for the deposition process.[44]

In the current work, we have used $SCCO_2$ as the carrier for conveying the organometallic precursor compounds to dendrimer-containing matrices, which were formed by covalent molecular assembly in $SCCO_2$. The functional property of the PAMAM-containing film as a sequestering agent for nanoparticles is demonstrated by the introduction of copper acetylacetonate complex ($Cu(acac)_2$) in $SCCO_2$ and subsequently reducing the complex to form metallic nanoparticles. We have compared the properties of the films with those obtained by introducing precursors in a liquid solvent (tetrahydrofuran (THF)).

2. Experimental Section

2.1. Materials. Pyromellitic dianhydride (PMDA), second generation of polyamidodiamine dendrimer (PAMAM), copper acetylacetonate ($(Cu(acac)_2$) (all from Aldrich), 3-cyanopropyltrichlorosilane (CPS, Lancaster), and 4,4′-diaminodiphenylether (DDE, Fluka) were used as received. Trifluoroacetic anhydride (from Aldrich), carbon dioxide (SOXAL Code P40J purified grade with <20 ppm of H_2O), toluene, *N*,*N*-dimethylacetamide (DMAc), tetrahydrofuran (THF), and chloroform (all from Merck) were used directly without further purification. Silicon wafers (Well bond Manufacturing Services Pte Ltd., Singapore) were 0.6 mm thick, polished on one side and with a natural oxide layer. Quartz slides were purchased from Achema Co., Singapore.

2.2. Surface Modification. Quartz slides and silicon wafers were prepared and derviatized as stated elsewhere.[42,43] Briefly, they were cleaned with piranha solution, rinsed with deionized (DI) water and methanol in succession, and blown dry with nitrogen. (***Caution!*** *Piranha solution is highly corrosive. Extreme care should be taken when handling piranha solution, and only small quantities should be prepared.*) They were then immersed in a 3 mM CPS solution in distilled chloroform, rinsed thoroughly in chloroform, and dried in nitrogen. The cyano functional group at the free end of the silane was hydrolyzed to carboxylic acid by treatment with a solution of 1:1 (v/v) of concentrated sulfuric acid and deionized water at 110 °C for 2 h. The wafers were then rinsed in deionized water and dried in vacuum at 100 °C for 1 h.

2.3. Supercritical Fluid Processing. The SCF process was conducted in a system depicted in Chart 1. A 20 mm I.D. × 140 mm length stainless steel column was used to house the wafer samples as they were contacted with the depositing species in the presence of $SCCO_2$ at 40 °C and 10 MPa. The temperature was maintained by immersing the column in a constant temperature bath, and CO_2 was pressurized by means of an ISCO syringe pump. The depositing species and precursor were introduced into the $SCCO_2$ stream by means of an HPLC pump.

2.4. Surface Modification of Acid to Anhydride in $SCCO_2$. The carboxylic groups on the surface of the CPS-containing substrate were converted to anhydrides by injecting 100 μL of trifluoroacetic anhydride into the $SCCO_2$ stream via a six-way Valco valve. The $SCCO_2$ flow was maintained for 3 h before depressurization.

2.5. LbL Assembly in $SCCO_2$. The anhydride-derivatized substrates were placed in the stainless steel column and exposed to a flow of $SCCO_2$ at 10 MPa and 40 °C at a flowrate of 800 mL/min (ambient conditions). 100 μL of 3 mM PAMAM in DMAc was injected into the $SCCO_2$ stream. The $SCCO_2$ flow was maintained for 3 h before depressurization. PMDA dissolved in DMAc (1.5 mM) was metered into the $SCCO_2$ stream at 250 μL/min over a 2-h period. This was followed by deposition of the second PAMAM layer as described above. Finally, the column was flushed with pure $SCCO_2$ for 45 min before depressurization.

2.6. Introduction of Copper Precursor. 2.6.1. Conventional Process. The assembled films were immersed in a 1% $Cu(acac)_2$ solution (0.082 g in 10 mL of THF) for 24 h; and then the films were rinsed copiously in THF and dried. The effect of

Scheme 1. Schematic for the Nanoparticle Formation in the Molecular Assembly

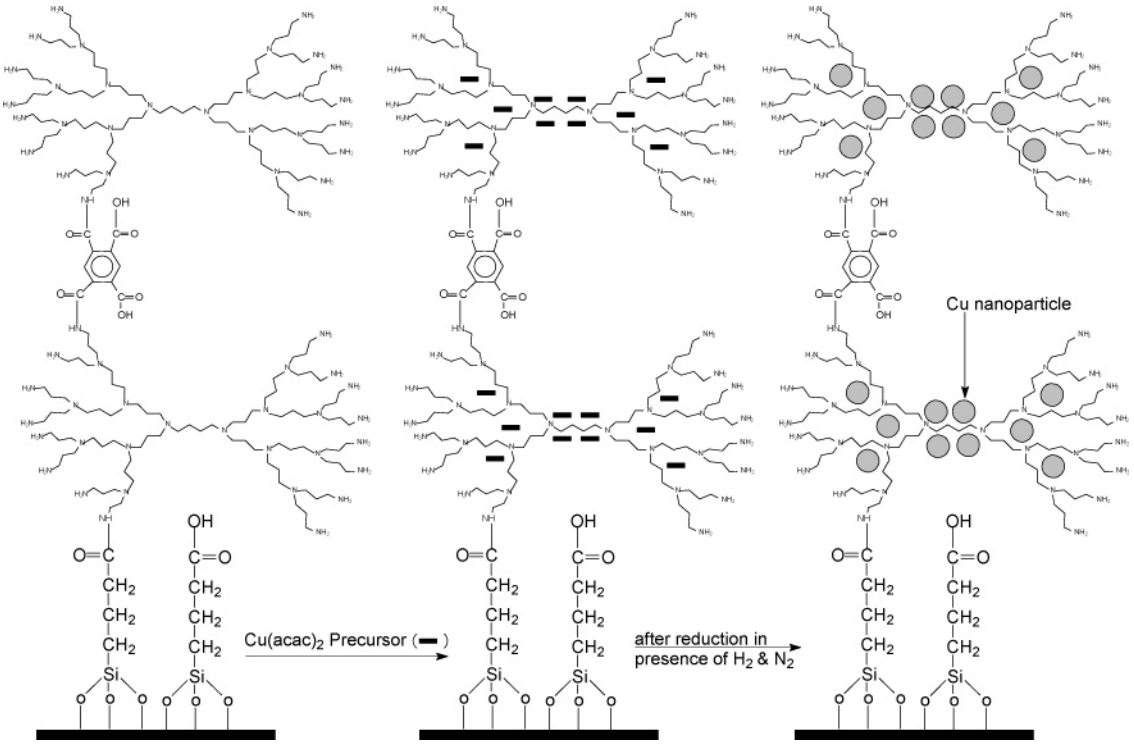

the solvent rinse subsequent to precursor introduction was investigated by reducing some precursor-laden films without the solvent rinse step.

2.6.2. SCF Process. Introduction of the nanoparticle precursor in the SCF medium was carried out by injecting 100 μL of 0.25% $Cu(acac)_2$ solution (0.0205 g in 10 mL of THF) into the high-pressure line at 10 MPa and 40 °C via the six-way valve. The column was flushed with pure $SCCO_2$ for 1 h after a 2-h exposure to the $Cu(acac)_2$ solution.

2.6.3. Reduction. The precursor-laden films were heated at 250 °C for 2 h in the presence of hydrogen and nitrogen (1:3 by volume) to decompose the acetylacetonate complex. By carrying out these steps sequentially, a nanoparticle-containing multilayer dendrimer film with a covalently linked −A−B−A−B− structure can be produced through amide and amic acid formation as shown in Scheme 1.

Given the low concentrations of the depositing species and precursor, and taking into consideration the measured solubilities of the precursor and DMAc in dense CO_2,[45,46] it is reasonable to assume that the contents of the column are homogeneous.

3. Characterization

X-ray photoelectron spectroscopy (XPS) measurements were made on a Kratos Analytical AXIS HSi spectrometer with a monochromatized Al Kα X-ray source (1486.71 eV photons) at a constant dwell time of 100 ms and pass energy of 40 eV. The core-level signals were obtained at a photoelectron takeoff angle of 90° (with respect to the sample surface). The X-ray source was run at a reduced power of 150 W. The pressure in the analysis chamber was maintained at 7.5×10^{-9} Torr or lower during each measurement.

The surface morphology of the films was examined by AFM (atomic force microscopy; NanoScope IVa, Digital Instruments). All images were collected in air using the tapping mode and a monolithic silicon tip. The drive frequency was 330 ± 50 kHz, and the voltage was between 3.0 and 4.0 V. The drive amplitude was about 300 mV, and the scan rate was 0.5−1.0 Hz.

Film thickness and refractive index characterization were performed by ellipsometry (Wvase 32, Woollam). Scanning spectra were acquired over the wavelength range of 600−1000 nm at three different incidence angles, 65°, 70°, and 75°. The model for the thin film measurement used silicon (Si.MAT) as the base layer with 1 mm thickness, silicon dioxide (SiO2.MAT) as the next layer with a thickness of 2.5−3 nm, and the Cauchy package (CAUCHY.MAT) for the film material. The mean-squared error values were less than 2 after fitting, indicating reliability of the model and the measurement.

UV−visible spectra were obtained on a Shimadzu UV-1601 PC scanning spectrometer within the range of 200−600 nm to monitor the growth of the film. A clean bare quartz slide was used as reference.

Transmission electron microscope (TEM) images of the composite ultrathin films deposited on gold grids were obtained with a JEM-2010 TEM (JEOL) operated at 120 kV. The dendrimer films on the surface of a gold TEM grid (3 mm diameter with 100 mesh) were prepared in the same manner as those on Si or quartz slides, except that the surface modifier for gold was 3-mercaptopropanoic acid. The surface derivatization was completed by acid-to-anhydride conversion and was followed by dendrimer and PMDA deposition (in succession), all carried out in $SCCO_2$. The size of the nanoparticles in the TEM images was measured manually to calculate the size distribution.

The EDS (energy dispersive spectroscopy) studies of the composite film samples were carried out on a JSM (5600LV) SEM (scanning electron microscopy) instrument. The films were sputter-coated with platinum metal to prevent charging of the sample by the electron beam.

4. Results and Discussion

4.1. X-ray Photoelectron Spectroscopy. The XPS scans for copper (Cu 2p) for samples formed by different processing methods (Figure 1) are presented in the energy range of 925−

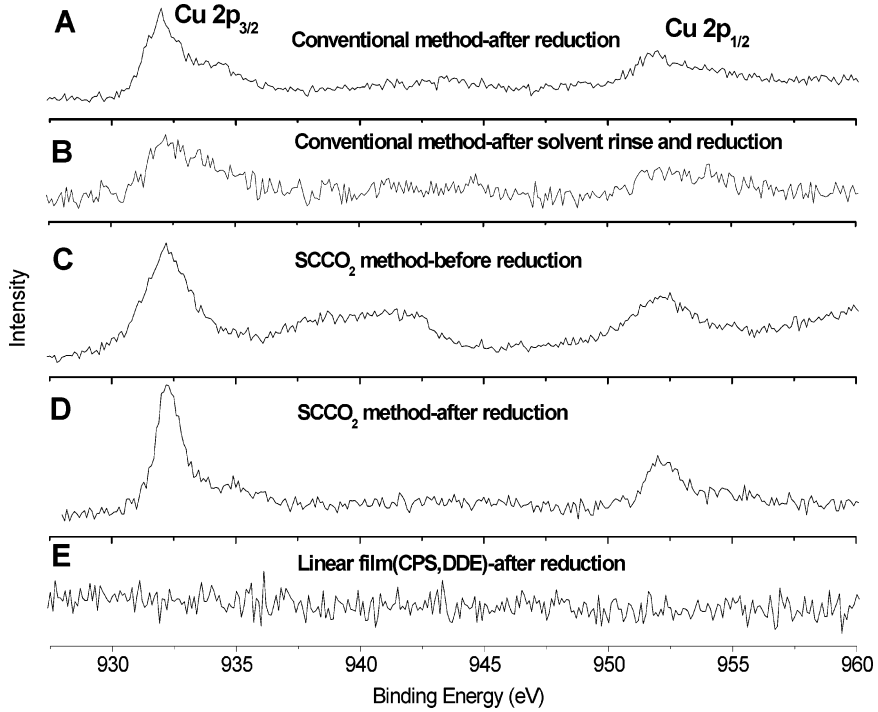

Figure 1. XPS wide scans for samples from different processing methods. (A) Precursor introduced in THF and sample reduced without solvent rinse; (B) precursor introduced in THF and sample reduced with solvent rinse; (C) precursor introduced in $SCCO_2$ and sample scanned before reduction; (D) sample (C) after reduction; and (E) dendrimer-free assembly (CPS/DDE) after reduction.

980 eV, in the immediate vicinity of the Cu 2p levels, localized at the 932.6 eV ($2p_{3/2}$) and 953 eV ($2p_{1/2}$) binding energies for metallic copper. The binding energy for Cu^+ in copper oxide is 932.5 eV ($2p_{3/2}$), which is very close to that for the metallic copper (932.6 eV, $2p_{3/2}$). The position of the absorption peak ($2p_{3/2}$) is at the binding energy of 932.6 eV, and none of the satellite structure associated with Cu^{2+} is observed in the spectra; this suggests that Cu^{2+} species are not present in the film. The Cu 2p spectra on the surface suggest that Cu species are present here in either the +1 or the 0 valence state because the +1 valence state cannot be ruled out unambiguously on the basis of XPS data.[47]

The intensities of the Cu XPS peaks for the conventionally formed film (spectrum A, Figure 1) decrease when the subsequent solvent rinse was performed on it (spectrum B, Figure 1). On the other hand, a higher intensity was observed in the SCF film (Figure 1, spectrum C before reduction and spectrum D after reduction) when compared to that for the conventionally formed film. This suggests that processing in the supercritical phase has resulted in a higher yield of nanoparticles than when liquid solvents were employed.

To verify whether the presence of the dendrimer is advantageous to nanoparticle formation and retention, we introduced $Cu(acac)_2$ as a precursor into the CPS/DDE/PMDA/DDE oligoimide film (i.e., in the absence of the dendrimer) using $SCCO_2$, and subsequently reduced the precursor in the H_2–N_2 mixture. The diamino diphenyl ether (DDE) was used as a bifunctional amine in the place of the dendrimer. XPS results show a very small peak for Cu, indicating the presence of a negligible amount of Cu nanoparticles when compared to dendrimer-containing films (spectrum E, Figure 1). This indicates that the presence of the dendrimer is crucial to ensure the retention of the precursor and subsequent formation of the nanoparticles in the films encapsulated within the dendrimer matrix.

The total concentration of the Cu particles after reduction was calculated from XPS elemental analysis. It has been observed that the total concentration of the Cu particles is 3 times higher than that of the THF processed film after rinsing with the solvent.

4.2. Surface Morphology. The AFM images (Figure 2) obtained after completion of the processing and the thermal reduction show distinct differences in the surface morphology based on the processing medium and method. The presence of nanoparticles on the surface is observed when the precursor is introduced using THF without the subsequent rinse step (Figure 2A and A′). However, if the precursor introduction (using THF) is followed by rinse in THF (Figure 2B and B′), a featureless, smeared out topography is observed, suggesting that the rinse step has washed away most of the (presumably) loosely tethered precursor. In the case where the precursor is introduced in $SCCO_2$ (Figure 2C and C′), the density of nanoparticles has increased relative to that observed in Figure 2A and A′. It is important to note that the $SCCO_2$ process has a built-in rinse step in the sense that the precursor-laden samples are flushed with pure $SCCO_2$ prior to depressurization. Therefore, we observe that the partitioning of the precursor between THF and the film appears to be in favor of the former medium, while that between $SCCO_2$ and the film is advantageous to the latter.

The differences in number density of particles may be related to the differences in uptake, transport, and retention of $Cu(acac)_2$ by the different processing methods. Introduction of precursors in the SCF medium offers advantages such as rapid solvent separation and transport (because of higher diffusivities and absence of surface tension) and the possibility that the depositing species can readily permeate into the voids of the dendrimer. Upon depressurization of the system, CO_2 rapidly escapes as a gas and the infused precursor is trapped inside the dendrimer. On the other hand, the lower diffusivity of conventional solvents may prevent the precursor material from accessing the void space of the dendrimer and the subsequent solvent rinse results in the loss of the physically adsorbed material. Therefore,

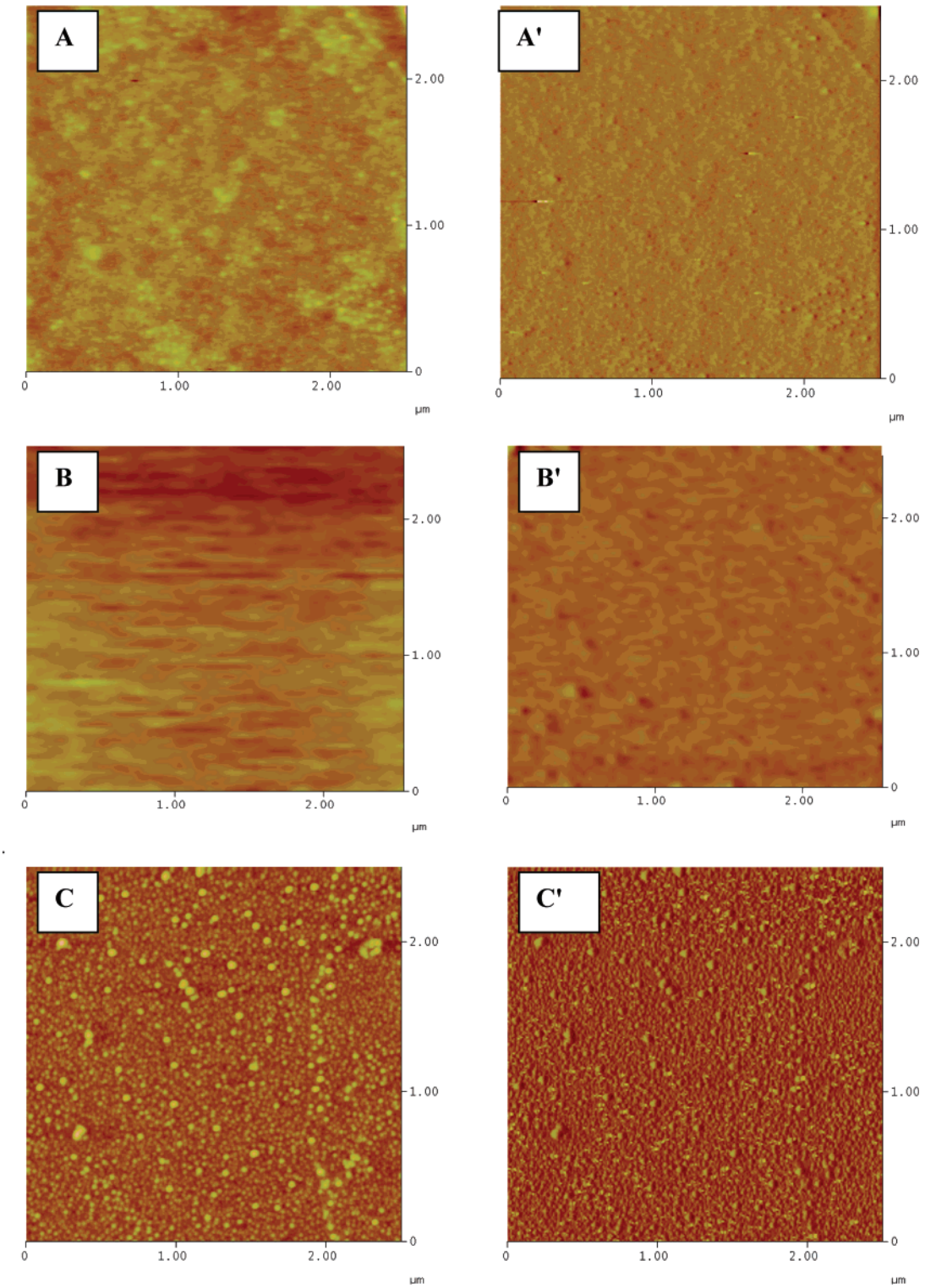

Figure 2. AFM height and phase images showing relative density of Cu nanoparticles obtained by different processing methods: (A (height) and A′ (phase)) conventional method after reduction; (B (height) and B′ (phase)) conventional method after solvent rinse and reduction; and (C (height) and C′ (phase)) SCF method after reduction.

processing in the supercritical phase results in a higher yield and a denser distribution of nanoparticles than when THF is employed.

Figure 3 presents the electron microscopy images and particle size distributions for Cu nanoparticles encapsulated within the dendrimer film formed by the SCF processing method. In these micrographs, Cu nanoparticles are seen as dark circular spots and the dendrimer matrices are indicated as gray patches. The TEM image (Figure 3, image A) shows that the particles are well separated. Figure 3 (image B) shows that the diameter of the nanoparticles obtained from the TEM images is 7 ± 3 nm (assuming the particles to be spherical). It is known that, among the factors that affect the size of encapsulated nanoparticles, the nature of the terminal groups of the dendrimers has an impact;[19] many metal precursors complex with the peripheral amines of amine-terminated dendrimers, forming metal clusters of sizes 5 nm and above, stabilized by multiple dendrimers.[20]

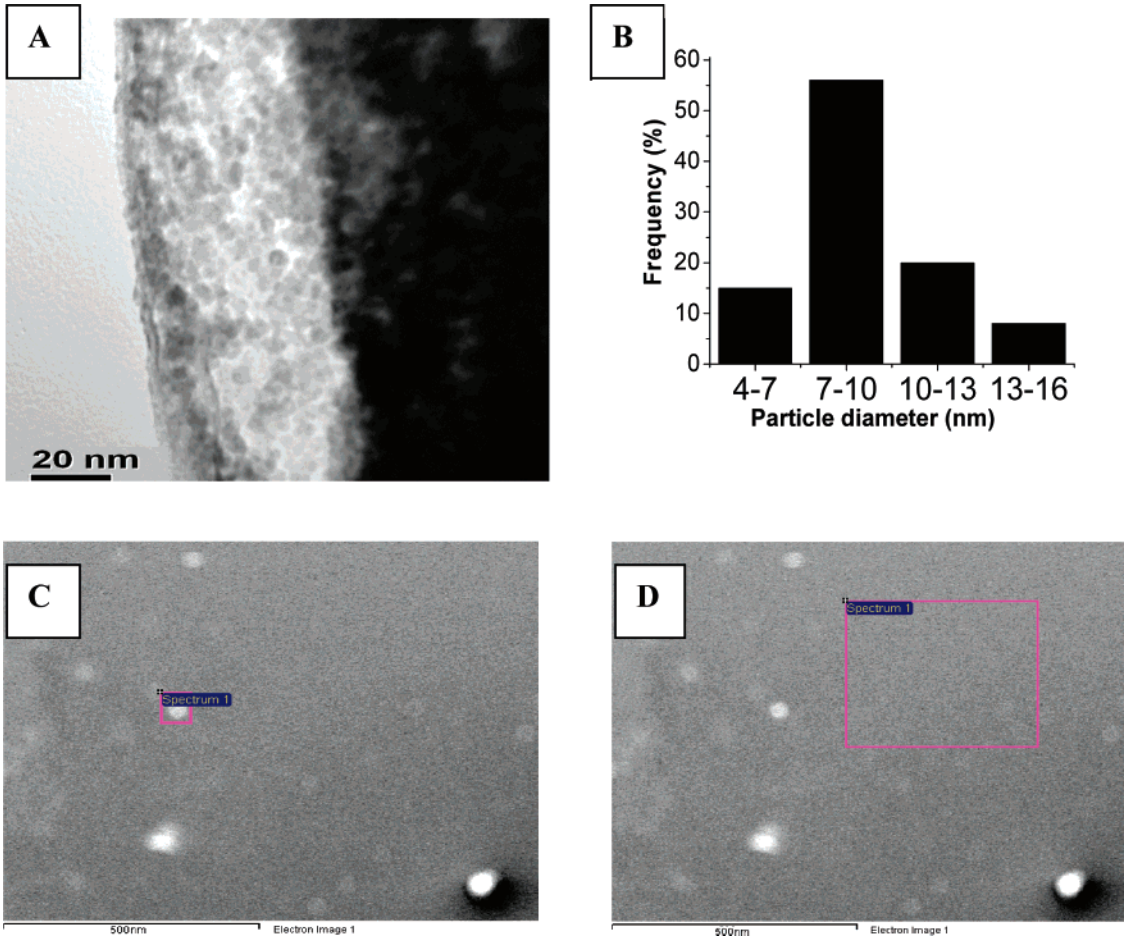

Figure 3. Electron microscopy for SCF-processed samples after reduction. TEM image (A) and the corresponding particle size distribution (B); SEM images (C and D). The average particle size and distribution were determined by measuring 100 metal nanoparticles.

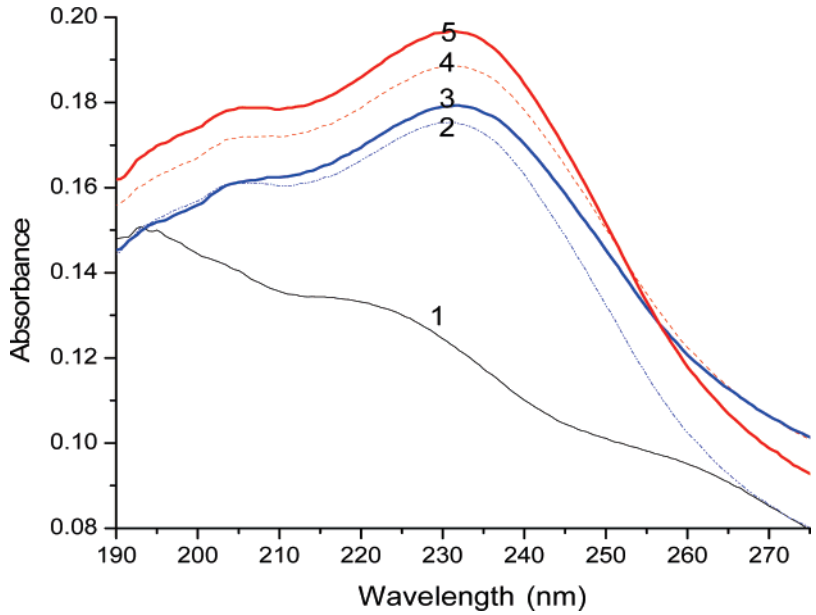

Figure 4. Comparison of UV−vis absorption spectra for encapsulated Cu nanoparticles in dendrimer film: (1) assembly of two dendrimer layers without nanoparticles; (2 and 3) nanoparticle-laden films with the precursor introduced in THF; (4 and 5) nanoparticle-laden films with the precursor introduced in SCF; and (2 and 4) after 24 h immersion in THF.

SEM-EDS analyses confirmed the presence of Cu as shown in Figure 3. Elemental Cu was found (image C) on the film in the bright spots, while Cu could not be observed outside of the spots (image D).

4.3. UV−Visible Absorption. From Figure 4, the presence of Cu in the film is inferred from the observation of a strong absorption peak at 230 nm arising from a ligand-to-metal charge-transfer (LMCT) transition within the dendrimer. Crooks et al.[12] and Tomalia et al.[17] have reported similar peaks for Cu−PAMAM nanocomposite solutions. This peak is not observed in the spectrum of the films prior to introduction of the precursor. Absorption at 230 nm in the film obtained with SCF

Table 1. Thickness and Refractive Index Values for Samples Formed by the Different Processing Methods

		thickness (nm)	refractive Index
sample A	dendrimer-containing film	7.1	0.71
sample B	after precursor introduction in THF	7.5	0.79
	after reduction	7.6	0.88
	after 24 h immersion in THF	7.5	0.81
sample C	after precursor introduction in THF, followed by solvent rinse	7.1	0.74
	after reduction	7.3	0.80
	after 24 h immersion in THF	7.2	0.77
sample D	after precursor introduction in $SCCO_2$	7.3	0.85
	after reduction	7.5	0.98
	after 24 h immersion in THF	7.3	0.95

processing is greater as compared to that obtained by the conventional method. This again suggests that more particles are formed by the SCF process.

To test their stabilities, conventional- and SCF-processed films on quartz slides were soaked in THF for 24 h after thermal reduction, and then blown dry with nitrogen. Both films show a decrease in UV−visible absorption intensity (Figure 4) after the immersion; however, the intensity of the SCF-processed film after the THF immersion is still higher than that of the THF-processed film prior to immersion in the solvent, thereby attesting to the increase in the presence of Cu nanoparticles despite exposure to the THF environment. While it is known that acetylacetonates have an affinity toward amine under certain conditions,[48,49] the above observations suggest that interaction between amines and acetylacetonates is enhanced in the absence of a conventional solvent. Furthermore, the greater density of nanoparticles obtained by using $SCCO_2$ suggests that the process is more efficient, because a smaller amount of precursor material was used relative to that used in THF processing.

4.4. Ellipsometry. Table 1 shows the ellipsometry results for different stages and modes of processing. The refractive index for the film progressively increases from 0.71 prior to precursor introduction to higher values after thermal reduction, indicating the presence of the Cu species in the films. The effects of processing medium and solvent rinse are also evident from the refractive indices. The highest refractive index value is observed in the SCF-processed film; the values obtained for the THF-processed films are lower. Thus, the refractive index values corroborate with AFM and XPS results, suggesting that a higher yield and denser distribution of particles are obtained when processing in $SCCO_2$.

The refractive indices measured before and after the 24-h THF immersion also corroborate the inferences from absorption spectra. The THF-processed film undergoes the largest decrease in refractive index after the THF immersion, indicating removal of substantial amount of nanoparticles. The decrease is less for the THF-processed film that has been subjected to the THF rinse due to the earlier removal of unbound precursor during the rinse step. The highest post-immersion value of refractive index is observed for the SCF-processed film. The smaller reduction in refractive index and thickness values for the latter suggests that the encapsulated film structure formed in SCF still remains largely intact upon polar solvent attack when compared to that formed in THF. The film thickness for all of the differently processed films shows a common trend, increase in thickness (or swelling) upon precursor introduction, a small, additional increase upon reduction due to formation of nanoparticles, and a decrease after the THF immersion step due to loss of material.

5. Conclusions

We have successfully demonstrated the feasibility of forming nanoparticles within covalently bonded multilayered dendrimer ultrathin films using supercritical carbon dioxide as a processing medium. Processing in the supercritical phase resulted in a higher yield and a denser and more stable distribution of nanoparticles than when a liquid solvent was employed, possibly due to facile solvent separation and transport. Formation of Cu nanoparticles within the dendrimer films is confirmed by XPS, AFM, TEM, UV−visible absorption spectroscopy, and ellipsometry. The SCF-processed film exhibited good stability toward polar solvent attack when compared to the THF-processed film.

Acknowledgment

We thank the National University of Singapore for providing financial support for this project and a research scholarship for S.R.P.

Literature Cited

(1) Murray, C. B.; Kagan, C. R.; Bawendi, M. G. *Annu. Rev. Mater. Sci.* **2000**, *30*, 545.

(2) Crooks, R. M.; Zhao, M.; Sun, L.; Chechick, V.; Yeung, L. K. *Acc. Chem. Res.* **2001**, *34*, 181.

(3) Templeton, A. C.; Zamborini, F. P.; Wuelfing, W. P.; Murray, R. W. *Langmuir* **2000**, *16*, 6682.

(4) Schmid, G.; Baümle, M.; Beyer, N. *Angew. Chem., Int. Ed.* **2000**, *39*, 181.

(5) Malynych, S.; Luzinov, I.; Chumanov, G. *J. Phys. Chem. B* **2002**, *106*, 1280.

(6) Freeman, R. G.; Grabar, K. C.; Allison, K. J.; Bright, R. M.; Davis, J. A.; Guthrie, A. P.; Hommer, M. B.; Jackson, M. A.; Smith, P. C.; Walter, D. G.; Natan, M. J. *Science* **1995**, *267*, 1629.

(7) Hu, K.; Brust, M.; Bard, A. J. *Chem. Mater.* **1998**, *10*, 1160.

(8) Musick, M. D.; Keating, C. D.; Lyon, L. A.; Botsko, S. L.; Peña, D. J.; Holliway, W. D.; McEvoy, T. M.; Richardson, J. N.; Natan, M. J. *Chem. Mater.* **2000**, *12*, 2869.

(9) Harnisch, J. A.; Pris, A. D.; Porter, M. D. *J. Am. Chem. Soc.* **2001**, *123*, 5829.

(10) Chan, E. W. L.; Yu, L. *Langmuir* **2002**, *18*, 311.

(11) Scott, R. W. J.; Datye, A. K.; Crooks, R. M. *J. Am. Chem. Soc.* **2003**, *125*, 3708.

(12) Lemon, B. I.; Crooks, R. M. *J. Am. Chem. Soc.* **2000**, *122*, 12886.

(13) Zhao, M.; Sun, L.; Crooks, R. M. *J. Am. Chem. Soc.* **1998**, *120*, 4877.

(14) Zhao, M.; Crooks, R. M. *Adv. Mater.* **1999**, *11*, 217.

(15) Esumi, K.; Suzuki, A.; Yamahira, A.; Torigoe, K. *Langmuir* **2000**, *16*, 2604.

(16) Esumi, K.; Hosoya, T.; Suzuki, A.; Torigoe, K. *J. Colloid Interface Sci.* **2000**, *226*, 346.

(17) Balogh, L.; Tomalia, D. A. *J. Am. Chem. Soc.* **1998**, *120*, 7355.

(18) Floriano, P. N.; Noble, C. O.; Schoonmaker, J. M.; Poliakoff, E. D.; McCarley, R. L. *J. Am. Chem. Soc.* **2001**, *123*, 10545.

(19) Gröhn, F.; Bauer, B. J.; Akpalu, Y. A.; Jackson, C. L.; Amis, E. J. *Macromolecules* **2000**, *33*, 6042.

(20) Manna, A.; Imae, T.; Aoi, T. K.; Okada, M.; Yogo, T. *Chem. Mater.* **2001**, *13*, 1674.

(21) He, J. A.; Valluzzi, R.; Yang, K.; Dolukhanyan, T.; Sung, C.; Kumar, J.; Tripathy, S. K. *Chem. Mater.* **1999**, *11*, 3268.

(22) Luo, Y.; Li, Y.; Jia, X.; Yang, H.; Yang, L.; Zhou, Q.; Wei, Y. *J. Appl. Polym. Sci.* **2003**, *89*, 1515.

(23) Oh, S. K.; Kim, Y. G.; Ye, H.; Crooks, R. M. *Langmuir* **2003**, *19*, 10420.

(24) Gallymov, M. O.; Vinokur, R. A.; Nikitin, L. N.; Said Galiv, E. E.; Khokhlov, A. R.; Yaminsky, I. V.; Schaumburg, K. *Langmuir* **2002**, *18*, 6928.

(25) Said Galiv, E.; Nikitin, L.; Gallymov, M.; Kurykin, M.; Petrova, O.; Lokshin, B.; Volkov, I.; Khokhlov, A.; Schaumburg, K. *Ind. Eng. Chem. Res.* **2000**, *39*, 4891.

(26) Said Galiv, E. E.; Vygodskki, Y. S.; Nikitin, L. N.; Vinokur, R. A.; Gallymov, M. O.; Khokhlov, A. R. *Polym. Sci., Ser. B* **2001**, *43*, 227.

(27) Weinstein, R. D.; Yan, D.; Jennings, G. K. *Ind. Eng. Chem. Res.* **2001**, *40*, 2046−2053.

(28) Yan, D.; Jennings, G. K.; Weinstein, R. D. *Ind. Eng. Chem. Res.* **2002**, *41*, 4528.

(29) (a) Fulton, J. L.; Pfund, D. M.; Romack, T. J.; Combes, J. R.; Samulski, E. T.; DeSimone, J. M.; Capel, M. *Langmuir* **1995**, *11*, 4241. (b) McClain, J. B.; Betts, D. E.; Canelas, D. A.; Samulski, E. T.; DeSimone, J. M.; Londono, J. D.; Cochran, H. D.; Wignall, G. D.; Chillura-Martino, D.; Triolo, R. *Science* **1996**, *274*, 2049. (c) Buhler, E.; Dobrynin, A. V.; DeSimone, J. M.; Rubinstein, M. *Macromolecules* **1998**, *31*, 7347.

(30) Shah, P. S.; Husain, S.; Johnston, K. P.; Korgel, B. A. *J. Phys. Chem. B* **2001**, *105*, 9433.

(31) Kameo, A.; Yoshimura, T.; Esumi, K. *Colloids Surf., A* **2003**, *215*, 181.

(32) Watkins, J. J.; McCarthy, T. J. *Chem. Mater.* **1995**, *11*, 1991.

(33) Watkins, J. J.; McCarthy, T. J. *J. Polym. Mater. Sci. Eng.* **1995**, *73*, 158.

(34) Watkins, J. J.; McCarthy, T. J. *J. Polym. Mater. Sci. Eng.* **1996**, *74*, 402.

(35) Rosolosky, J.; Boggess, R. K.; Rubira, A. F.; Taylor, L. T.; Stokley, D. M.; St. Clair, A. K. *J. Mater. Res.* **1997**, *12*, 3127.

(36) Boggess, R. K.; Taylor, L. T.; Stokley, D. M.; St. Clair, A. K. *J. Appl. Polym. Sci.* **1997**, *64*, 1309.

(37) Nazem, N.; Taylor, L. T.; Rubira, A. F. *J. Supercrit. Fluids* **2002**, *23*, 43.

(38) Morley, K. S.; Marr, P. C.; Webb, P. B.; Berry, A. R.; Allison, F. J.; Moldovan, G.; Brown, P. D.; Howdle, S. M. *J. Mater. Chem.* **2002**, *12*, 1898.

(39) Yoda, S.; Hasegawa, A.; Suda, H.; Uchimaru, Y.; Haraya, K.; Tsuji, T.; Otake, K. *Chem. Mater.* **2004**, *12*, 2363.

(40) (a) Brennecke, J. F. *Nature* **1997**, *389*, 333. (b) Cooper, A. I.; Londono, J. D.; Wignall, G.; Mcclain, J. B.; Samulski, E. T.; Lin, J. S.; Dobrynin, A.; Rubinstein, M.; Burke, A. L. C.; Frechet, J. M. J.; Desimone, J. M. *Nature* **1997**, *389*, 360.

(41) Yijun, J.; Qiuming, G. *J. Am. Chem. Soc.* **2006**, *128*, 717.

(42) Puniredd, S. R.; Srinivasan, M. P. *Langmuir* **2005**, *21*, 7812.

(43) Puniredd, S. R.; Srinivasan, M. P. *Langmuir* **2006**, *22*, 4092.

(44) Puniredd, S. R.; Srinivasan, M. P. *J. Colloid Interface Sci.* **2006**, *306*, 118.

(45) Lagalante, A. F.; Hansen, B. N.; Bruno, T. J.; Sievers, R. E. *Inorg. Chem.* **1995**, *34*, 5781.

(46) Francis, A. W. *J. Phys. Chem.* **1954**, *58*, 1099.

(47) Pertsin, A. J.; Pashunin, Y. M. *Appl. Surf. Sci.* **1991**, *47*, 115.

(48) Silva, A. R.; Martins, M.; Madalena, M.; Freitas, A.; Figueiredo, J. L.; Freire, C.; De Castro, B. *Eur. J. Inorg. Chem.* **2004**, 2027.

(49) Jarrais, B.; Silva, A. R.; Freire, C. *Eur. J. Inorg. Chem.* **2005**, 4582.

Received for review June 27, 2006
Revised manuscript received October 25, 2006
Accepted October 28, 2006

IE060822Q